Adsorption (2014) 20:905–915
DOI 10.1007/s10450-014-9635-7

Adsorption equilibrium and kinetics of cesium onto insoluble Prussian blue synthesized by an immediate precipitation reaction between Fe^{3+} and $[Fe(CN)_6]^{4-}$

Hirotaka Fujita · Hiromi Sasano · Risa Miyajima · Akiyoshi Sakoda

Received: 16 May 2014 / Revised: 2 September 2014 / Accepted: 4 September 2014 / Published online: 12 September 2014

Abstract The adsorption equilibrium and kinetics of cesium ion (Cs^+) onto insoluble Prussian blue (PB) prepared by an immediate precipitation reaction between Fe^{3+} and $[Fe(CN)_6]^{4-}$ was investigated under initial Cs^+ concentration of under 0.15 mmol/L. Synthesis conditions in this method were almost insensitive to the adsorption ability of insoluble PB, and this method provided one of the smallest PB crystallites among synthesis methods. Even when molar concentration of H_3O^+ was more than 200 times higher or molar concentration of K^+ was more than 50,000 times higher than that of Cs^+ in the aqueous solution, the equilibrium adsorption amount was reduced by only approximately one-half to two-third of that in the pure system; that is, the insoluble PB synthesized possessed a considerably high adsorption selectivity for Cs^+. In contrast to the excellent adsorption ability under adsorption equilibrium, adsorption rate was quite slow. It took at least 2 weeks at 25 °C to completely attain the adsorption equilibrium, even though the primary particle size (crystallite size) and secondary particle size (aggregate size of the crystallites) were sufficiently small at approximately 14 nm and 53–106 μm, respectively. This slow adsorption is primarily due to the large resistance of intracrystalline diffusion; the intracrystalline diffusion coefficient was extremely small at less than 3.3×10^{-22} m^2/s. We also found that increase in temperature could significantly decrease this diffusion resistance, resulting in much quicker elimination of Cs^+ from the aqueous solution.

Keywords Prussian blue · Adsorption · Cesium · Immediate precipitation reaction

1 Introduction

Prussian blue (PB) and its analogues have a high adsorption capacity and selectivity for cesium (Cs) (Thanapon et al. 2010; Mimura et al. 1997), and hence for decades have been recognized as an excellent remover of radioactive Cs. Since the accident at the Fukushima Daiichi power plant, PB has attracted increasing attention as a material for use in decontaminating the environment. PB can be categorized into two types in terms of its dispersibility in water and/or chemical composition: insoluble PB ($Fe(III)_4[Fe(II)(CN)_6]_3$; IPB) and soluble PB ($KFe(III)[Fe(II)(CN)_6]$; SPB) (Buser et al. 1977; Louise et al. 2013; Itaya et al. 1986; Keggin and Miles 1936). PB is generally produced from a mixture of Fe^{3+} and $[Fe(II)(CN)_6]^{4-}$ aqueous solutions or a mixture of Fe^{2+} and $[Fe(III)(CN)_6]^{3-}$ aqueous solutions. IPB is synthesized under conditions in which Fe^{3+} or Fe^{2+} is in excess of $Fe(II)(CN)_6^{4-}$ or $Fe(III)(CN)_6^{3-}$ in the solution, while SPB is synthesized under conditions in which $Fe(II)(CN)_6^{4-}$ or $Fe(III)(CN)_6^{3-}$ is in excess of Fe^{3+} or Fe^{2+} (Louise et al. 2013; Richard et al. 1970). They differ in terms of how colloidal they appear in the aqueous solution (Buser et al. 1977; Louise et al. 2013). As their names suggest, SPB has higher dispersibility in water (Buser et al. 1977; Louise et al. 2013), and hence, the IPB seems to be more advantageous for the adsorption process, because IPB is easier to recover after the adsorption by solid/liquid separation. In addition, there are various kinds of synthesis

H. Fujita (✉) · A. Sakoda
Institute of Industrial Science, University of Tokyo, 4-6-1 Komaba, Meguro-ku, Tokyo 153-8505, Japan
e-mail: fujiozon@iis.u-tokyo.ac.jp

H. Sasano · R. Miyajima
School of Science and Technology, Meiji University, 1-1-1 Higashimita, Tama-Ku, Kawasaki, Kanagawa 214-8571, Japan

methods for PB, including: (1) immediate precipitation reaction between Fe^{3+} and $M_4[Fe(CN)_6]$ (Louise et al. 2013; Pawel 1990; Gotoh et al. 2007; Ishizaki et al. 2013); (2) oxidation of Berlin white synthesized by the mixing of Fe^{2+} and $M_4[Fe(II)(CN)_6]$ aqueous solutions (Louise et al. 2013); and (3) hydrothermal synthesis from $M_4[Fe(II)(CN)_6]$ (Wu et al. 2006; Hu et al. 2009) or $M_3[Fe(III)(CN)_6]$ (Zheng et al. 2007; Torad et al. 2012). (M is the alkali cation or NH_4^+.) By employing these synthesis methods, PB with different morphology and crystallite size can be prepared.

Some information regarding the adsorption properties of Cs^+ onto PB and its analogues is available in the literature (Thanapon et al. 2010; Mimura et al. 1997; Hu et al. 2009; Torad et al. 2012, Faustino 2008). However, the ability of PB to adsorb Cs^+ varies considerably according to its origin such as what synthesis method was used, and under what conditions the PB was prepared. For example, Ishizaki et al. reported that the adsorption equilibrium differed significantly between PB synthesized by the immediate precipitation reaction and that commercially available (Ishizaki et al. 2013). Torad et al. demonstrated that adsorption capacity varied considerably according to both the morphology of the PB and the surface area (Torad et al. 2012). Also, in terms of adsorption kinetics, the period that it takes to completely attain the adsorption equilibrium has been reported to range from several hours to several months (Thanapon et al. 2010; Mimura et al. 1997; Ishizaki et al. 2013; Torad et al. 2012; Faustino 2008; Ayrault et al. 1998) Furthermore, in many cases, reports do not include information regarding which PB (IPB or SPB) was used. Thus, it is very important to systematically summarize the relationship between the adsorption ability of PB and its origin, elucidating the detailed structure of the PB employed, in order to better understand what type or structure of PB has the best adsorption abilities including adsorption equilibrium and kinetics.

For this purpose, we aimed to study the adsorption ability of Cs^+ onto IPB synthesized by the conventional precipitation reaction between Fe^{3+} and $[Fe(CN)_6]^{4-}$ as the first step. Among various synthesis methods, the immediate precipitation method is one of the simplest and the most orthodox. However, the fundamentals of adsorption of Cs^+ onto IPB synthesized by this method have not been elucidated clearly. Ishizaki et al. discussed the mechanism of Cs^+ adsorption using IPB synthesized by the immediate precipitation (Ishizaki et al. 2013). However, the reports included little information with regard to the adsorption ability of Cs^+ in the presence of high concentrations of other competitive cations like H_3O^+, K^+, etc. Also, information has been quite limited with regard to adsorption kinetics onto IPB synthesized by this method in the literature.

Therefore, the objective of this study was to elucidate adsorption equilibrium and kinetics of Cs^+ onto IPB synthesized by the conventional method using the immediate precipitation reaction between Fe^{3+} and $[Fe(CN)_6]^{4-}$ using non-radioactive Cs^+.

2 Experiment

2.1 Synthesis of IPB by immediate precipitation reaction

IPB was prepared under three conditions in which Fe^{2+} or Fe^{3+} was in excess of $Fe(II)(CN)_6^{4-}$ or $Fe(III)(CN)_6^{3-}$ in the synthesis solution, as shown in Table 1. The aqueous solution (A) was added drop-wise into the aqueous solution (B) using a peristaltic pump at ambient temperature in order to obtain the precipitate of IPB. The precipitated IPB in the solution was separated by centrifugal separation, and then rinsed with approximately 100 cc of ion-exchanged water. This combination of centrifugal separation and rinse was repeated 6 times, and the IPB obtained was then dried on a hot plate at 40 °C. The IPB appeared as crystallite-aggregated grains (Gotoh et al. 2007) several millimeters in diameter. Obtained IPB samples were then crushed by mortar and classified by stainless sieves into smaller particles with a suitable diameter before each experiment. In this study, IPB-1 was mainly used in the experiments, while others were used mainly for comparison. All the chemicals used were purchased from Wako.

2.2 Characterization of IPB

SEM (Scanning electron microscope) observation was performed with SEMS-4500 (HITACHI). The powder X-ray diffraction (XRD) pattern of the synthesized IPB was recorded on a diffractometer with Cukα radiation (RINT-2000, RIGAKU). Organic and inorganic element analysis was performed with a CHN analyzer (PE2400 series CHNS/O analyzer, Perkin Elmer) and an energy dispersive

Table 1 Synthesis condition of IPB

	Aqueous solution (A)	Aqueous solution (B)
IPB-1	1.36×10^{-2} mol-$K_4[Fe(CN)_6]\cdot 3H_2O$/L (300 mL)	1.77×10^{-2} mol-$FeCl_3$/L (600 mL)
IPB-2	1.36×10^{-1} mol-$K_4[Fe(CN)_6]\cdot 3H_2O$/L (300 mL)	1.77×10^{-1} mol-$FeCl_3$/L (600 mL)
IPB-3	1.36×10^{-2} mol-$K_3[Fe(CN)_6]$/L (300 mL)	1.77×10^{-2} mol-$FeCl_2\cdot 4H_2O$/L (600 mL)

X-ray fluorescence (XRF) spectrometer (EDX-800, Shimadzu), respectively. Thermogravimetric analysis was also performed using TGA (DTG-60, Shimadzu) with flowing 100 cc/min of air.

2.3 Adsorption experiment of Cs^+

Synthesized IPB was added to 500 cc of aqueous solution containing Cs^+ ranging from 0 to 0.15 mmol-Cs^+/L, and then a batch adsorption experiment was started with shaking at the rate of 150 rpm. The ratio of solution volume to weight of IPB added ranged from 10 to 30 L/g. In order to examine the influence of coexisting cation such as H_3O^+ or K^+, HCl or KCl was also added to the solution and dissolved completely before the adsorption experiment as necessary. The adsorption amount was calculated by one of the following two methods:

2.3.1 Case (A): in the absence of coexisting KCl in the aqueous solution

Cs^+ concentration in the supernatant was measured by high-performance liquid chromatography (HPLC) with a conductivity detector (CDD-10A, Shimadzu), and adsorption amount was calculated by the following equation:

$$q(t) = \frac{\mathrm{V(Co - C(t))}}{w} \quad (1)$$

where q(t) is the adsorption amount of Cs^+ [mmol/g], V is the volume of the aqueous solution [L], C_0 is the initial Cs^+ concentration in the aqueous solution [mmol/L], C(t) is the Cs^+ concentration when the sampling of the supernatant is carried out [mmol/L], w is the weight of PB added [g], and t is the elapsed time when the sampling was performed.

2.3.2 Case (B): in the presence of KCl in the aqueous solution

If the concentration of coexisting K^+ was higher than 0.77 mmol/L, the measurement of Cs^+ concentration in the supernatant was difficult under our measuring procedure because the peak of K^+ completely overlapped with that of Cs^+ in the HPLC chart. Hence, the PB after the adsorption experiment was filtered and rinsed with a small amount of ion-exchanged water. The obtained IPB-1 was dried at 40 °C, then subjected to inorganic elemental analysis by XRF to calculate the adsorption amount of Cs^+, as explained in detail later. Also, the equilibrated concentration of Cs^+ in the solution was calculated from this adsorption amount by following Eq. (2), which is a transformation of Eq. (1):

$$C(t) = C_0 - \frac{wq(t)}{V} \quad (2)$$

3 Results and discussion

3.1 Characterization of IPB-1

3.1.1 Composition

From the CHN analysis, the weight composition of C, H, and N were 17.2, 2.93, and 19.4 wt%, respectively. Also, the thermogravimetric analysis and XRF analysis showed that 48 wt% of the initial weight of IPB-1 was left as an inorganic ash after the temperature was increased to 500 °C (data not shown), and that the inorganic element of the ash was composed of over 98 mol % of Fe. Oxygen can't be detected by the energy dispersive XRF. Assuming that the ash was composed of only Fe_2O_3 (Zboril et al. 2004), the chemical formula of IPB-1 synthesized was determined as $Fe_{1.436}[Fe(CN)_6]\cdot 7H_2O$ (exp.: Fe 32.5 wt% C 17.2 wt% N 19.4 wt% H 2.93 wt%, calc.: Fe 32.5 wt% C 17.2 wt% N 20.1 wt% H 3.35 wt%), which is close to that of IPB reported in the literature ($Fe_4[Fe(CN)_6]_3\cdot XH_2O$) (Buser et al. 1977; Louise et al. 2013).

3.1.2 Particle structure

Figure 1 shows an example of an SEM image of IPB-1. Several 100 μm of particles can be observed, and its surface is scabrous. However, it was not possible to obtain more detailed information on the nanostructure of IPB-1 from the SEM observation. Figure 2a shows the XRD pattern of IPB-1. The peaks shown were all ascribed to the Prussian blue, which had the cubic lattice (Buser et al. 1977; Louise et al. 2013; Keggin and Miles 1936), providing absolute evidence that PB was successfully synthesized. The structure of IPB, including atomic displacement of Fe, C, N, and O obtained by the Rietveld refinement, is described in detail elsewhere (Buser et al. 1977; Louise et al. 2013). As for the XRD analysis, the lattice constant and crystallite size were calculated after background subtraction by the Sonneveld–Visser method (Sonneveld and Visser 1975) and removal of kα2 contribution with the assumption that the peak intensity ratio of Kα1/Kα2 was 0.5. The lattice constant was calculated as 1.015 nm by the extrapolation method using Nelson–Riley function (Nntsott 1945), as shown in Fig. 2b. Various values have been reported for the lattice constant of PB in the literature, ranging from 1.015 to 1.021 nm (Louise et al. 2013). Hence, the lattice constant seems to change a little according to the synthesis method and conditions. Furthermore, as shown in Fig. 2c, crystallite size was calculated as 14 nm using the W–H method (Georgea et al. 2011) where Lorentzian function was employed for peak fitting in this study. It has been reported that different sizes of crystallite, ranging from approximately 10 nm to several

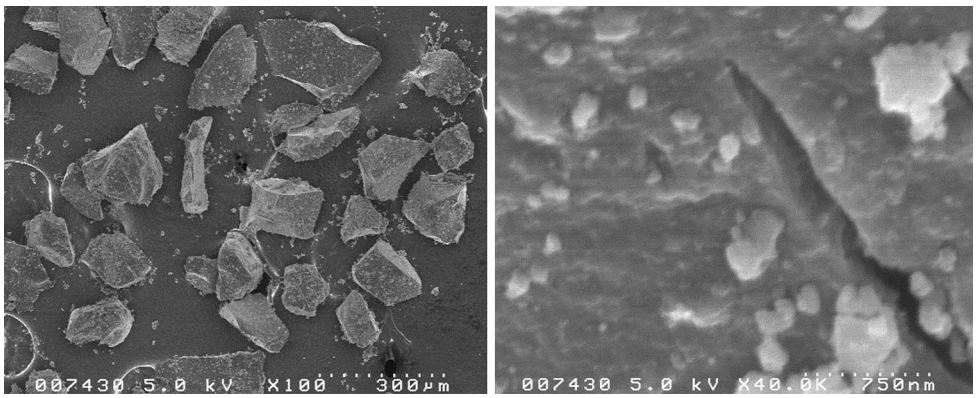

Fig. 1 SEM image of IPB-1 crushed and sieved into 106–200 μm

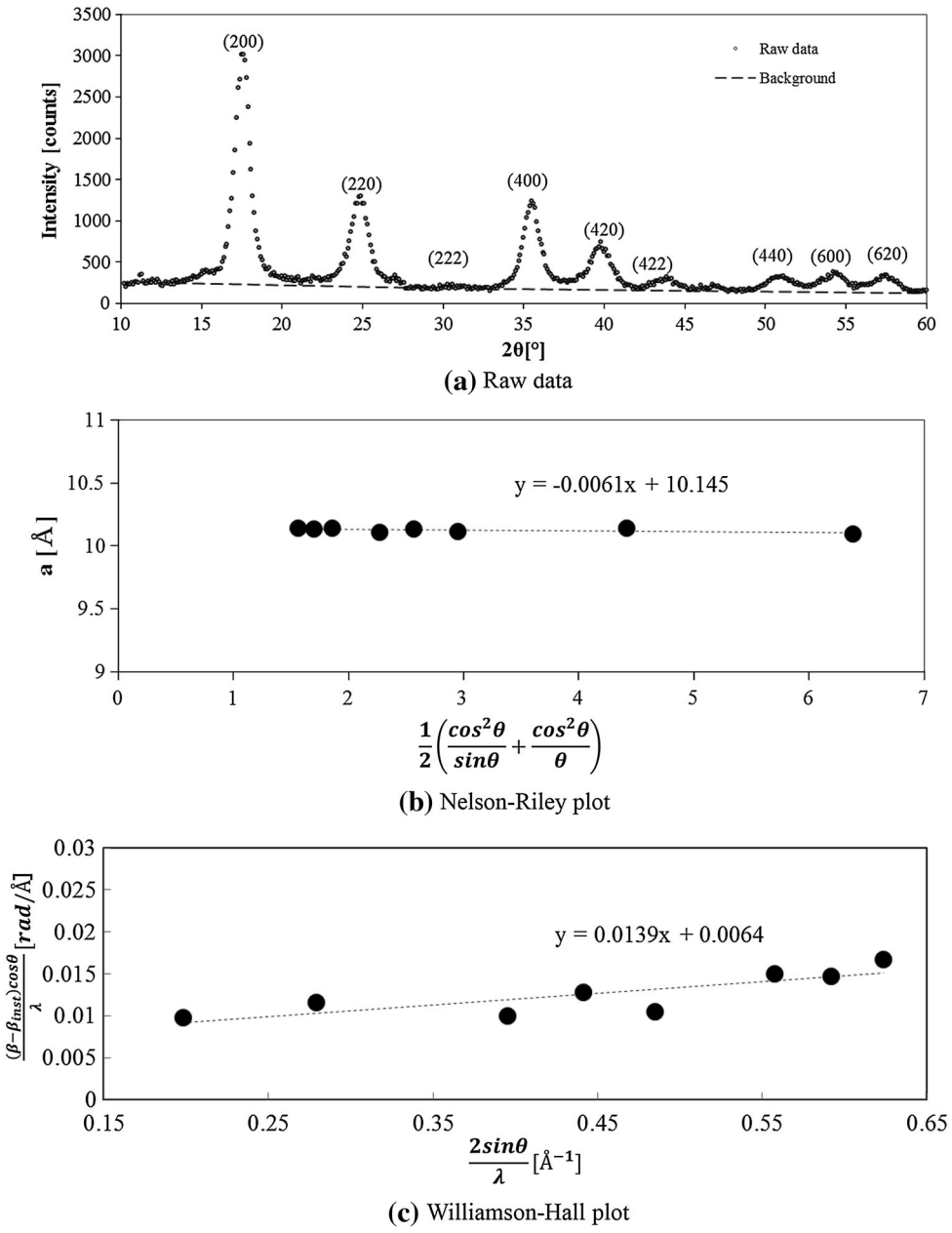

Fig. 2 XRD pattern of IPB-1 (a: lattice constant [Å], β: observed FWMH [rad], βinst: instrumental FWMH [rad])

Fig. 3 Particle structure of IPB

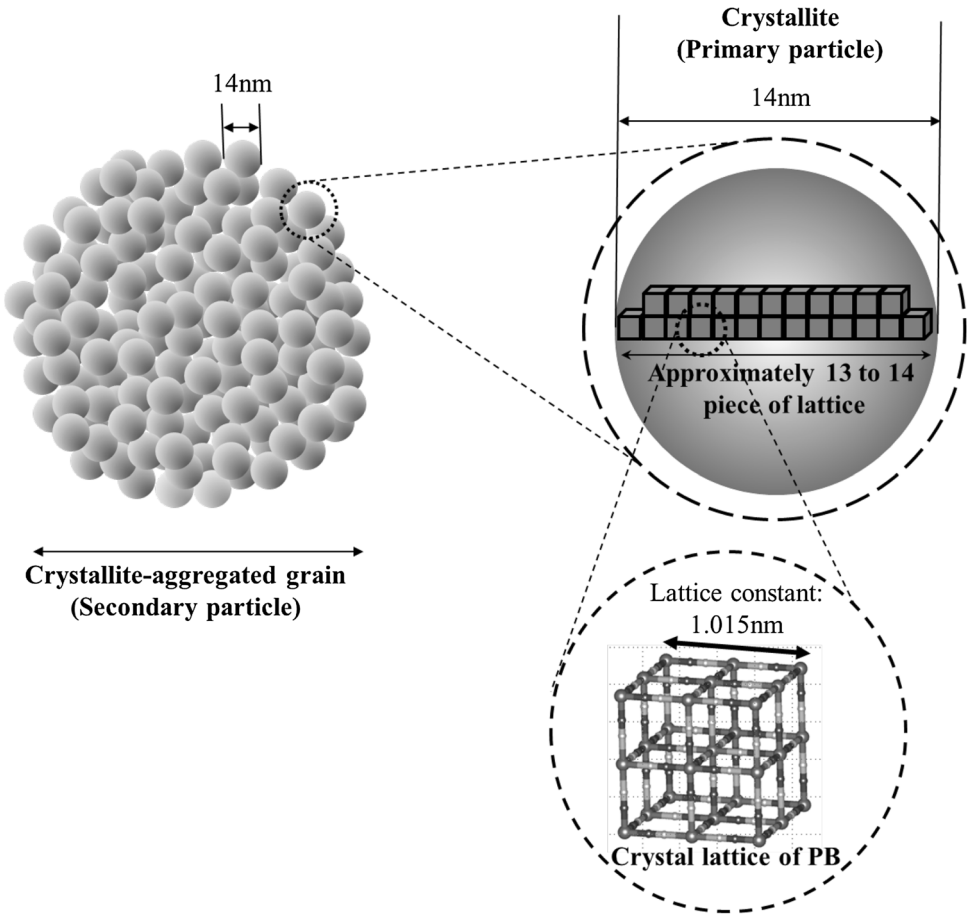

μm, can be synthesized under different synthesis methods and conditions (Louise et al. 2013). To the best of our knowledge, the literature indicates that this method provides one of the smallest PB crystallites. Gotoh et al. found that PB synthesized by the immediate precipitation to be approximately 10 nm in crystallite size, and that the diameter of PB particles directly observed by TEM was almost consistent with the crystallite size obtained by XRD analysis (Gotoh et al. 2007). This means that the primary particle of IPB-1 is the crystallite, and their aggregate forms a larger grain, i.e., a secondary particle (Gotoh et al. 2007). As a result, the particle structure of IPB-1 is hierarchical, as shown in Fig. 3.

3.2 Adsorption experiments

3.2.1 Correlation between the amount of Cs^+ adsorbed and the Cs/Fe ratio of the PB after the adsorption

As mentioned above, it is very difficult to measure Cs^+ concentration in the supernatant by HPLC when high concentrations of K^+ are present. Hence, the amount of Cs^+ adsorption was determined by inorganic elemental analysis of IPB using XRF after the adsorption experiment. To accomplish this, the relation between the amount of Cs^+ adsorbed and the Cs/Fe ratio of the IPB-1 was investigated in advance. Specially, the adsorption experiment was carried out first without K^+ in the solution, and then the amount of Cs^+ adsorbed was determined by the measurement of the initial and equilibrated Cs^+ concentrations in the supernatant by HPLC. Subsequently, the spent IPB-1 was recovered by filtration, and the Cs/Fe ratio was determined by XRF using the FP (fundamental parameter) method. Results indicated that the correlation between amount of Cs^+ adsorbed and the Cs/Fe ratio was completely linear, as shown in Fig. 4. This meant that the amount of Cs^+ adsorbed by IPB-1 could be accurately determined by the Cs/Fe ratio measured by XRF using this correlation, even in the presence of high concentrations of K^+ in the solution.

3.2.2 Adsorption equilibrium

Figure 5 shows the adsorption equilibrium Fig. 5a, b illustrate the influence of coexisting H_3O^+ and K^+ on the adsorption equilibrium, respectively. Even though molar concentration of H_3O^+ or K^+ was more than 200 times or

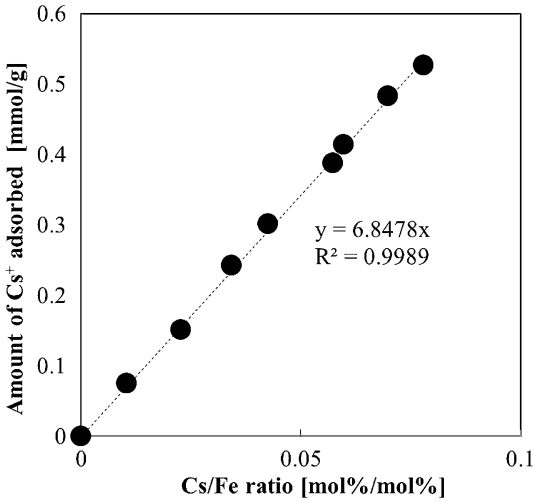

Fig. 4 Relationship between Cs/Fe ratio and amount adsorbed of Cs^+ (initial pH 5.6, coexisting K^+ concentration: 0 mmol/L, adsorbent: IPB-1)

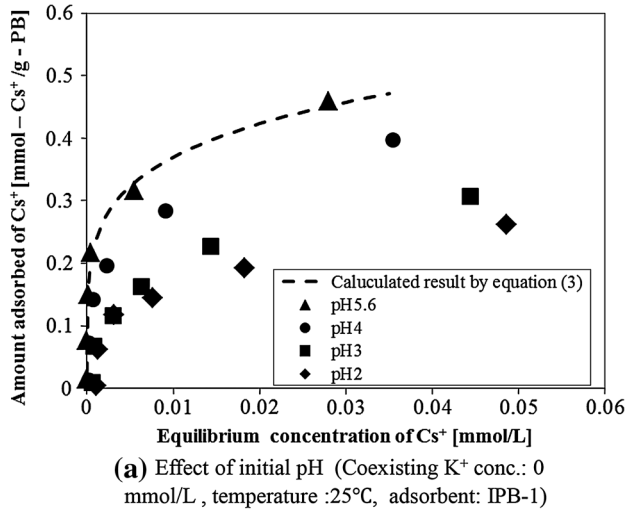

(a) Effect of initial pH (Coexisting K^+ conc.: 0 mmol/L , temperature :25°C, adsorbent: IPB-1)

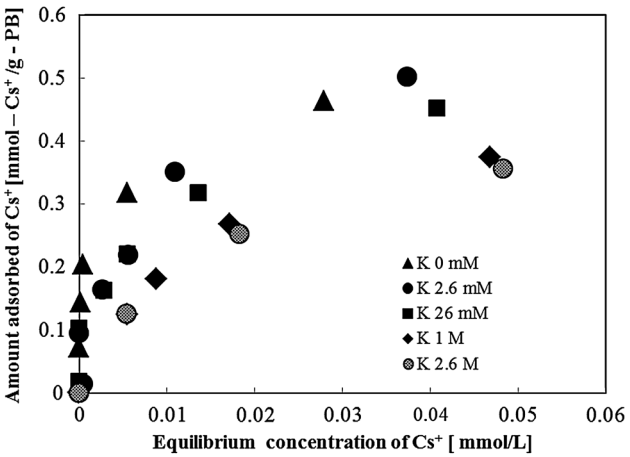

(b) Effect of initial K^+ concentration (Initial pH:5.6, temperature :25°C, adsorbent: IPB-1)

Fig. 5 Effect of pH and K^+ concentration on adsorption equilibrium of Cs^+ onto IPB-1

more than 50,000 times, respectively, that of Cs^+ in the aqueous solution, the equilibrium adsorption amount was only reduced approximately one-half to one-third of that in the absence of them, meaning the synthesized PB possessed an extremely high adsorption selectivity for Cs^+. Figure 6 shows the Cs/Fe and K/Fe ratio of IPB-1 after the adsorption experiment in the presence of high concentrations (1, 2.6 mol/L) of K^+ in the solution. As the initial concentration of Cs^+ in the solution increased, the Cs/Fe ratio of IPB-1 also increased, with (Cs + K)/Fe maintained at almost the same value. Here, it should be noted that the K/Fe ratio of as-synthesized IPB was under 0.02. This suggested that the IPB-1 was able to uptake both Cs^+ and K^+, and that competitive adsorption occurred at almost the same site of IPB-1 at this concentration range. Figure 7 shows the relationship between amount of Cs^+ adsorbed from the solution onto IPB-1 and that of H_3O^+ released from IPB-1 to the solution. The Cs^+ adsorption was measured by the HPLC of the supernatant, while the amount of H_3O^+ released was calculated from the difference in pH before and after the adsorption experiment. This result confirmed that these amounts are almost the same, although the amount of Cs^+ adsorbed was slightly larger than that of H_3O^+ released. The phenomenon of Cs^+ adsorption onto PB accompanying the H_3O^+ release from IPB has also been qualitatively confirmed in the literature (Ishizaki et al. 2013; Faustino 2008). Our result provided quantitative evidence that the adsorption of Cs^+ onto insoluble PB prepared by the precipitation method occurred mainly via ion exchange between Cs^+ with H_3O^+, which originally resided in the IPB. As a result of Rietveld refinement of PB synthesized by the immediate precipitation reaction, the main adsorption site is considered to be located near the center of subcubic cell of the crystal lattice (Moritomo and Tanaka 2013). However, the reason why this site can selectively adsorb Cs^+ remains unclear, and further detailed study of the structure of PB before and after adsorption is needed for its elucidation.

3.2.3 Adsorption kinetics

The dependence of adsorption rate on the secondary particle size is shown in Fig. 8. (We emphasize here that the secondary particle size is not the crystallite size but the size of the crystallite-aggregated grain.) Regardless of its secondary particle size, it took more than 2 weeks to completely reach the adsorption equilibrium. In the literature, time taken to reach the adsorption equilibrium of Cs^+ onto PB or its analogue was reported to range from several hours to several months (Thanapon et al. 2010; Mimura

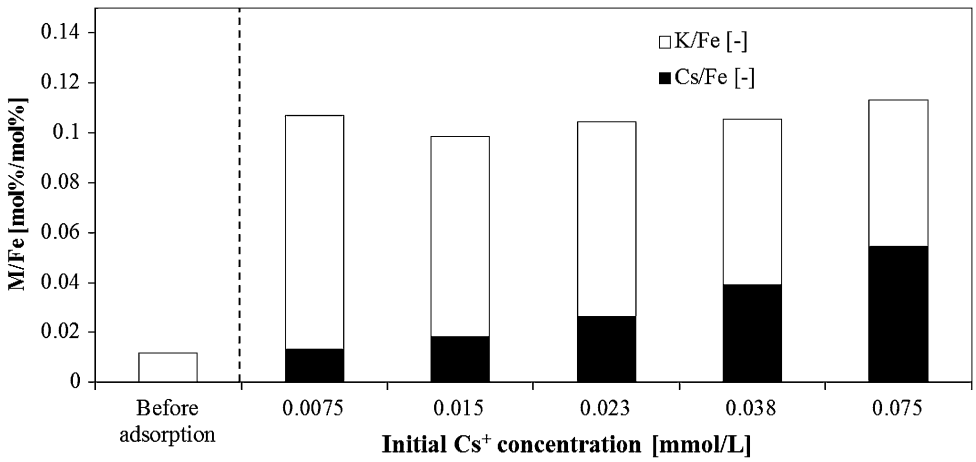

(a) Coexisting K^+ conc.: 1000 mmol/L

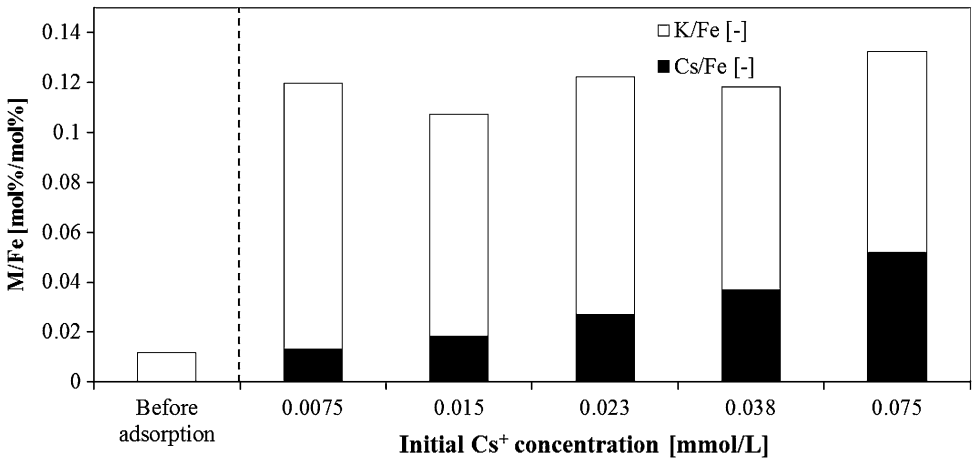

(b) Coexisting K^+ conc.: 2600 mmol/L

Fig. 6 K/Fe and Cs/Fe ratios after adsorption experiment of Cs^+ under coexistence of high concentration of K^+ (initial pH 5.6, V/w = 10L/g, M: Alkali cation (Cs^+ or K^+))

et al. 1997; Ishizaki et al. 2013; Torad et al. 2012; Faustino 2008; Ayrault et al. 1998). It can be said that the adsorption rate of Cs^+ onto IPB-1 is quite slow. Taking the particle structure shown in Fig. 3 into consideration, adsorption is considered to occur via diffusion at the external surface of the crystallite-aggregated grains, that at the interfaces between the crystallites (intercrystalline diffusion) and that in the genuine pore network (intracrystalline diffusion) (Steffen et al. 2013), and there is a possibility that one of these is a rate-limiting step. We found that dynamic adsorption behavior depended little on secondary particle size, as shown in Fig. 8. This fact suggested that intracrystalline diffusion is likely to be close to rate-limiting step under our experimental conditions (Suzuki 1990a). Assuming this, adsorption kinetics were analyzed using the following equations and the boundary condition (Suzuki 1990b; Kärger and Ruthven 1992).

$$q = kc^{\frac{1}{n}} \tag{3}$$

$$\frac{\partial q}{\partial t} = D_i\left(\frac{\partial^2 q}{\partial r_i^2} + \frac{2}{r_i}\frac{\partial q}{\partial r_i}\right) \tag{4}$$

$$\frac{\partial c}{\partial t} = -\frac{3w}{r_i V} D_i \left(\frac{\partial q}{\partial r_i}\right)_{r_i = R_{io}} \tag{5}$$

$$t = 0 \rightarrow c = C_0, \quad q = q_0 \tag{6}$$

where q is the adsorption amount of Cs^+ [mmol/g], k and n are the Freundlich constants, c is the concentration of Cs^+ in the solution [mmol/L], D_i is the intracrystalline diffusion coefficient [m^2/s], w is the weight of IPB-1 added into the solution [g], and V is the volume of solution [L], t is the adsorption time [s], C_0 is the initial concentration, q_o is the amount of Cs^+ adsorbed when the equilibrium concentration of Cs^+ in the solution is C_0, r_i is the length from the center of the PB crystallite (assumed to be a sphere), and R_{io} is the radius of the crystallite. It was confirmed in advance that the adsorption equilibrium without K^+ in the solution could be expressed by the Freundlich equation (k

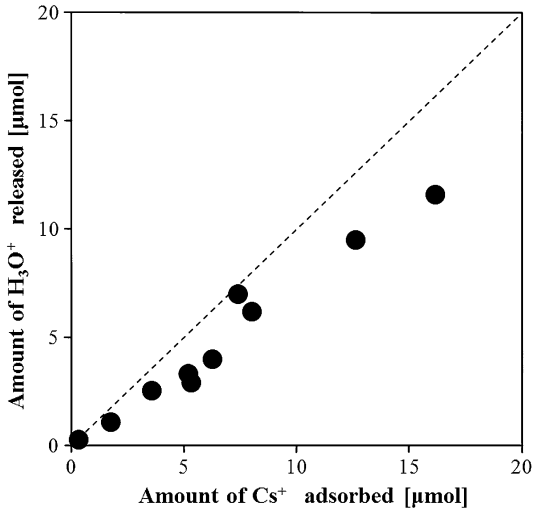

Fig. 7 Relationship between amount of Cs^+ adsorbed and that of H_3O^+ released to the liquid phase (initial pH 5.6, initial K^+ concentration: 0 mg/L, initial Cs^+ concentration: 0–0.075 mmol/L, V/w: 10 L/g, adsorbent: IPB-1)

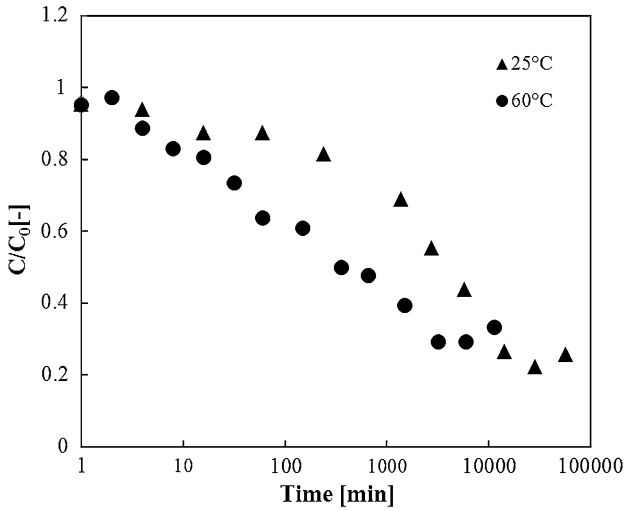

Fig. 9 Effect of temperature on dynamic adsorption behavior of Cs onto IPB-1 (initial pH 5.6, initial K^+ concentration: 0 mmol/L, initial Cs^+ concentration: 0.0226 mmol/L, adsorbent: IPB-1, secondary particle size: 53–106 μm

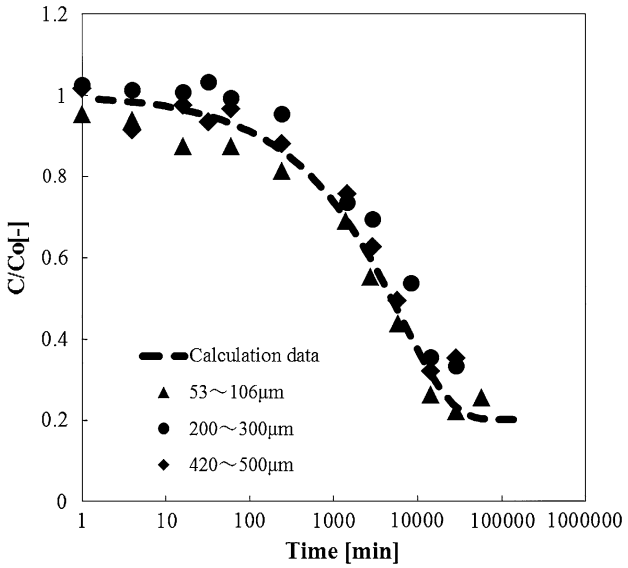

Fig. 8 Dynamic adsorption behavior of Cs onto IPB-1 with different size of secondary particle (initial pH 5.6, temperature: 25 °C, initial K^+ concentration: 0 mmol/L, initial Cs^+ concentration: 0.0226 mmol/L, adsorbent: IPB-1)

and n were 0.903 and 5.16, respectively), as shown in Fig. 5a As a result of the nondimensionalization of these equations, D_i/R_{io}^2 is the value to be determined (Suzuki 1990b; Kärger and Ruthven 1992). The series of Eqs. (3)–(5) was solved numerically using Fortran 95. The validity of the numerical solution was also confirmed in advance by comparing the solution diagram and the obtained numerical solution. Here, we must mention that we didn't investigate the dependence of Cs^+ concentration on the adsorption rate in this study, although the set of equations implies the Cs^+ diffusivities to be independent of the concentration. The value of D_i/R_{io}^2 was determined by fitting the calculation curve to the experimental data. As shown in Fig. 8, a good agreement between calculation and experimental data was obtained when the D_i/R_{io}^2 was 6.7×10^{-6} [s^{-1}]. Also, if we assume that the Cs^+ can completely penetrate to the center of the crystallite, the D_i is calculated as 3.3×10^{-22} m^2/s, considering diffusion length was the same with R_{io} (7 nm). However, some groups insisted that adsorption was likely to occur only near the surface in some cases of adsorption onto Prussian blue analogues (Ayrault et al. 1998; Torad et al. 2012; Yang et al. 2014). If the penetration of Cs^+ did not reach the center of crystallite, the value of D_i could be less than the above value. Also, considering that the lattice constant is 1.015 nm, and that the crystallite size is 14 nm, it takes more than 2 weeks for Cs^+ to penetrate through only less than 6 or 7 crystal lattice at 25 °C. This meant that diffusion through each lattice was extremely slow. Moritomo et al. insisted that the potential curves of large cations including Cs^+ exhibit a barrier at the window of the host framework of Prussian blue analogues (Moritomo and Tanaka 2013). There is a possibility that this barrier at the window leads to quite slow diffusion. We again emphasize that the immediate precipitation reaction provided one of the smallest crystallites of PB. This suggests that the time constant of adsorption will be much larger—or deep penetration of Cs^+ into the PB crystallite will be practically impossible—in the case of PB with much larger crystallite

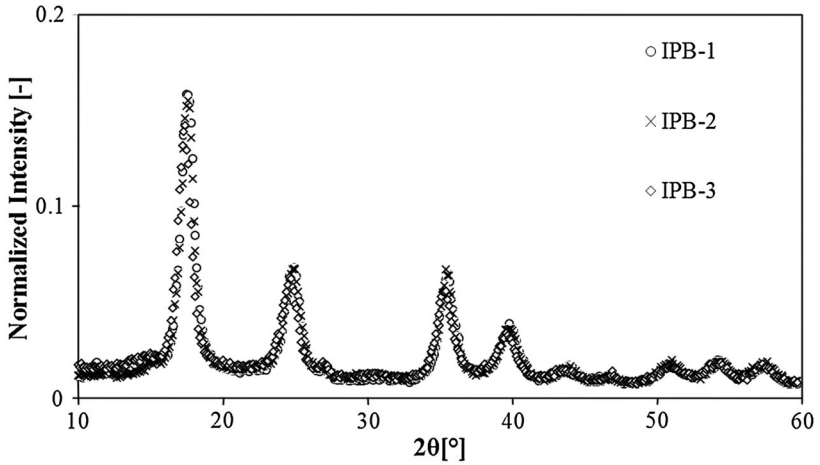

(a) XRD patterns of IPB-1, IPB-2,and IPB-3

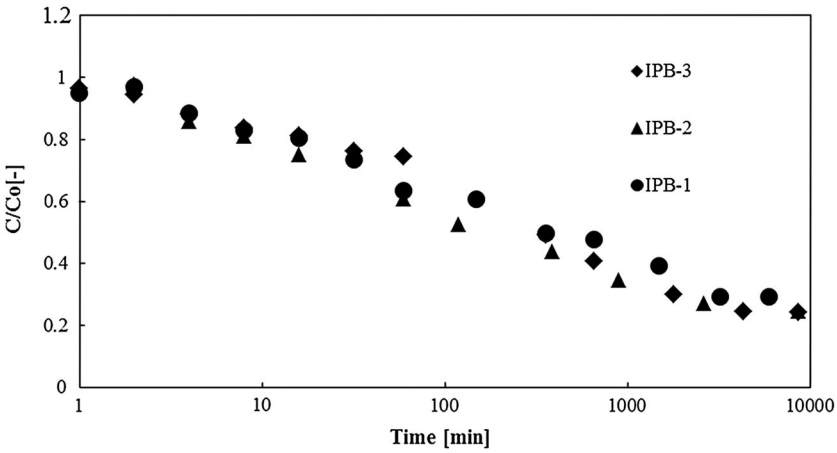

(b) Dynamic adsorption behaviors of IPB-1, IPB-2, and IPB-3 at 60° C
(Initila pH: 5.6, initial K^+ concentration: 0 mmol/L initial Cs^+ concentration:0.0226 mmol/L, secondary particle size: 53-106μm)

Fig. 10 XRD patterns and adsorption behaviors of IPBs synthesized by the immediate precipitation reaction under different conditions

size prepared by other synthesis methods. This topic will be addressed in future research.

Furthermore, Fig. 9 shows the effect of temperature on dynamic adsorption behavior. The adsorption equilibrium seemed to have little sensitivity to temperature, because the C/C_0 converged to almost the same value under the adsorption equilibrium regardless of temperature, as can be seen in Fig. 9. In contrast, we found that an increase of only 35 °C could increase the adsorption rate significantly; at 60 °C, it took only 2 days to attain the adsorption equilibrium. This suggested that the activation energy of intracrystalline diffusion is very large, as well as that a little temperature increase can decrease intracrystalline diffusion resistance significantly (Steffen et al. 2013). To the best of our knowledge, this study is the first to find this significant dependence of adsorption kinetic on temperature.

3.2.4 *Effect of synthesis condition of insoluble PB on adsorption of Cs^+*

From the literature, the adsorption ability of PB appears to differ significantly according to its origin. Hence, we must discuss the generalizability and applicability of the data obtained in this study. To accomplish this, the adsorption ability of IPB synthesized under different conditions was compared among IPB-1, IPB-2 and IPB-3. We found that dynamic adsorption behaviors at 60 °C were almost the same, as shown in Fig. 10b. Also, the peak broadenings of XRD patterns were almost the same, as shown in Fig. 10a, meaning they have almost the same crystallite size. From the comparison between IPB-1 and IPB-2, the concentrations of Fe^{3+} and $K_4[Fe(II)(CN)_6]$ had little or no influence on the adsorption behavior of IPB at 60 °C. Also, PB synthesized by a mixture of Fe^{3+} and $[Fe(II)(CN)_6]^{4-}$

(IPB-1 and IPB-2) is generally called "Prussian blue", while the PB synthesized by mixture of Fe^{2+} and $[Fe(III)(CN)_6]^{3-}$ (IPB-3) is called "Turnbull's blue". Many authors concluded that insoluble Prussian blue and Turnbull's blue were the same compounds (Ito et al. 1968); this study also confirmed that their adsorption abilities were almost the same at 60 °C. These results suggested that the synthesis condition of IPB in this method had little or no effect on the adsorption ability of IPB under the conditions used in this study. We emphasize again that neither adsorption ability nor crystallite size will be the same if a synthesis method other than that dealt in this study is used.

4 Conclusion

IPB prepared by the immediate precipitation reaction between Fe^{3+} and $[Fe(CN)_6]^{4-}$ possessed a considerably high adsorption selectivity for Cs^+. In contrast to the excellent adsorption ability under adsorption equilibrium, adsorption rate was quite slow. This slow adsorption is primarily due to the large resistance of intracrystalline diffusion; the intracrystalline diffusion coefficient was extremely small at less than 3.3×10^{-22} m^2/s. Also, we found that the temperature increase could significantly decrease the diffusion resistance, resulting in much quicker adsorption at relatively high temperature.

References

Ayrault, S., Jimenez, B., Garnier, E., Fedoroff, M., Jones, D.J., Loos-Neskovic, C.: Sorption mechanisms of cesium on $CuII_2$-$FeII(CN)_6$ and $CuII_3[FeIII(CN)_6]_2$ hexacyanoferrates and their relation to the crystalline structure. J. Solid State Chem. **141**(2), 185–475 (1998)

Buser, H.J., Schwarzenbach, D., Petter, W., Ludi, A.: The crystal structure of Prussian blue: $Fe_4[Fe(CN)_6]_3 \cdot xH_2O$. Inorg. Chem. **16**(11), 2704–2710 (1977)

Faustino, P.J., Yang, Y., Progar, J.J., Brownell, C.R., Sadrieh, N., May, J.C., Leutzinger, E., Place, D.A., Duffy, E.P., Houn, F., Loewke, S.A., Mecozzi, V.J., Ellison, C.D., Khan, M.A., Hussain, A.S., Lyon, R.C.: Quantitative determination of cesium binding to ferric hexacyanoferrate: Prussian blue. J. Pharm. Biomed. Anal. **47**(1), 114–125 (2008)

Georgea, A., Sharmaa, S.K., Chawlab, S., Malika, M.M., Qureshia, M.S.: Detailed of X-ray diffraction and photoluminescence studies of Ce doped ZnO nanocrystals. J. Alloy. Compd. **509**, 5942–5946 (2011)

Gotoh, A., Uchida, H., Ishizaki, M., Satoh, T., Kaga, S., Okamoto, S., Ohta, M., Sakamoto, M., Kawamoto, T., Tanaka, H., Tokumoto, H., Hara, S., Shiozaki, H., Yamada, M., Miyake, M., Kurihara, M.: Simple synthesis of three primary colour nanoparticle inks of Prussian blue and its analogues. Nanotechnology **18**, 345609–345615 (2007)

Hu, M., Jiang, J.S., Ji, R.P., Zeng, Y.: Prussian blue mesocrystals prepared by a facile hydrothermal method. CrystEngComm **11**, 2257–2259 (2009)

Ishizaki, M., Akiba, S., Ohtani, A., Hoshi, Y., Ono, K., Matsuba, M., Togashi, T., Kananizuka, K., Sakamoto, M., Takahashi, A., Kawamoto, T., Tanaka, H., Watanabe, M., Arisaka, M., Nankawad, T., Kurihara, M.: Proton-exchange mechanism of specific Cs^+ adsorption via lattice defect sites of Prussian blue filled with coordination and crystallization water molecules. Dalton Trans. **42**, 16049–16055 (2013)

Itaya, K., Uchida, I., Vernon, D.N.: Electrochemistry of polynuclear transition metal cyanides: Prussian blue and its analogues. Acc. Chem. Res. **19**(6), 162–168 (1986)

Ito, A., Suenaga, M., Ono, K.: Mössbauer study of soluble Prussian blue, insoluble Prussian blue, and Turnbull's blue. J. Chem. Phys. **48**, 3597–3599 (1968)

Kärger, J., Ruthven, D.M.: Diffusion in zeolite, pp. 230–244. Wiley, New York (1992)

Keggin, J.F., Miles, F.D.: Structures and formulæ of the Prussian blues and related compounds. Nature **137**, 577–578 (1936)

Louise, S., Fernande, G., Gary, J.L., Pauline, N., Pierre, B., David, S.: Relationship between the synthesis of Prussian blue pigments, their color, physical properties, and their behavior in paint layers. J. Phys. Chem. C **117**(19), 9693–9712 (2013)

Mimura, H., Lehto, J., Harjula, R.: Ion exchange of cesium on potassium nickel hexacyanoferrate(II). J. Nucl. Sci. Technol. **34**(5), 484–489 (1997)

Moritomo, Y., Tanaka, H.: Alkali cation potential and functionality in the nanoporous Prussian blue analogues. Adv. Condens. Matter Phys. **539620**, 9 (2013)

Nntsott, J.B., am Rrr rv, D.P.: An experimental investigation of extrapolation methods in the derivation of accurate unit-cell dimensions in crystals. Proc. Phys. Soc. **57**, 160–177 (1945)

Kulesza, P.J.: Solid-state electrochemistry of iron hexacyanoferrate (Prussian blue type) powders evidence for redox transitions in mixed-valence ionically conducting microstructures. J. Electroanal. Chem. **289**, 103–116 (1990)

Richard, E.W., Surendra, N.G., Billy, J.M.: Prussian blues. Inorg. Chem. **9**(11), 2512–2516 (1970)

Steffen, B., Frank, S., Helge, T., Dieter, F., Jörg, K., Jürgen, H.: Tracing water and cation diffusion in hydrated zeolites of type Li-LSX by pulsed field gradient NMR. J. Phys. Chem. C **117**(47), 24866–24872 (2013)

Sonneveld, E.J., Visser, J.W.: Automatic collection of powder data from photographs. J. Appl. Crystallogr. **8**, 1–7 (1975)

Suzuki, M.: Adsorption engineering, pp. 108–109. Kodansya, Tokyo (1990a)

Suzuki, M.: Adsorption engineering, pp. 95–98. Kodansya, Tokyo (1990b)

Thanapon, S., Vichaya, S., Robert, J.W., Rafal, M.G., Glen, E.F., Shane, A., Charles, T., Wassana, Y.: Selective capture of cesium and thallium from natural waters and simulated wastes, with copper ferrocyanide functionalized mesoporous silica. J. Hazard. Mater. **182**(1–3), 225–231 (2010)

Torad, N.L., Hu, M., Imura, M., Naito, M., Yamauchi, Y.: Large Cs adsorption capability of nanostructured Prussian blue particles with high accessible surface areas. J. Mater. Chem. **22**, 18261–18267 (2012)

Yang, H., Sun, L., Zhai, J., Li, H., Zhao, Y.A., Yu, H.: In situ controllable synthesis of magnetic Prussian blue/graphene oxide nanocomposites for removal of radioactive cesium in water. J. Mater. Chem. A **2**, 326–332 (2014)

Wu, X., Cao, M., Hu, C., He, X.: Sonochemical synthesis of Prussian blue nanocubes from a single-source precursor. Cryst. Growth Des. **6**(1), 26–28 (2006)

Zheng, X.J., Kuang, Q., Xu, T., Jiang, Z.Y., Zhang, S.H., Xie, Z.X., Huang, R.B., Zheng, L.X.: Growth of Prussian blue microcubes under a hydrothermal condition: possible nonclassical crystallization by a mesoscale self-assembly. J. Phys. Chem. C **111**, 4499–4502 (2007)

Zboril, R., Machala, L., Mashlan, M., Sharma, V.: Iron(III) oxide nanoparticles in the thermally induced oxidative decomposition of Prussian blue, $Fe_4[Fe(CN)_6]_3$. Cryst. Growth Des. **4**(6), 1317–1325 (2004)